ORIGINAL RESEARCH—BASIC

Proliferative Cell Targeting and Epithelial Cell Turnover Fuels Hepatitis E Virus Replication in Human Intestinal Enteroids



Nanci Santos-Ferreira,^{1,*} Xin Zhang,^{2,*} Laura Corneillie,³ Jana Van Dycke,¹ Winston Chiu,² Claire Montpellier,³ Johan Neyts,² Laurence Cocquerel,³ Suzanne J. F. Kaptein, and Joana Rocha-Pereira

 1 KU Leuven, Department of Microbiology, Immunology and Transplantation, Rega Institute, Virus-Host Interactions &Therapeutic Approaches (VITA) Research Group, Leuven, Belgium; ²KU Leuven, Department of Microbiology, Immunology and Transplantation, Rega Institute, Virology, Antiviral Drug & Vaccine Research Group, Leuven, Belgium; and ³Univ. Lille, CNRS, Inserm, CHU Lille, Institut Pasteur de Lille, U1019-UMR 9017-CIIL-Center for Infection and Immunity of Lille, Lille, France

BACKGROUND AND AIMS: Hepatitis E virus (HEV) is a leading pathogen causing acute viral hepatitis globally. While HEV is primarily spread fecal-orally, the role of the gut in HEV pathogenesis remains largely unexplored, including how HEV disseminates from gut to liver, and whether the gut is an HEV reservoir. We here aimed to illuminate HEV biology in the gut using human intestinal enteroids (HIEs). METHODS: Three strategies were explored to establish an HEV-HIE model three-dimensional (3D) HIEs, two-dimensional HIEs in transwell, and HEV RNA-electroporated HIEs. HEV particles produced by electroporated HIEs were characterized by western blot and gradient centrifugation. The intestinal tropism of HEV was investigated through confocal fluorescent microscopy and gene expression analysis. RESULTS: HEV infection in 3D-HIEs and two-dimensional-HIEs showed limited replication, whereas HIEs electroporation led to a sustained increase in the release of nonenveloped infectious virions. These virions could reinfect new 3D-HIEs, yielding a ~ 2 log₁₀ increase in HEV RNA over time. In electroporated HIEs, high expression of the infectious open reading frame 2 capsid form was observed in the supernatant. Importantly, 70% of all HEV-infected cells were identified as proliferative cells (leucine-rich-repeat-containing G-protein-coupled receptor 5 intestinal stem cells and transitamplifying progenitor cells). Open reading frame 2 staining was also observed in absorptive enterocytes, goblet, and enteroendocrine cells. CONCLUSION: Overall, we established a robust HEV-HIE model that yields high titers of infectious nonenveloped virions. Proliferative cells and the fast intestinal epithelial cell turnover are important features that facilitate efficient HEV replication, and likely also its dissemination. This study suggests that the gut is an HEV reservoir, capable of producing some of the nonenveloped HEV shed in the feces.

Keywords: Enteroendocrine cells; Hepatitis E virus; Human intestinal enteroids; Infection; Proliferating cells; Stem cells

Introduction

he enteric hepatitis E virus (HEV) poses a sub-transmitted fecal-orally, with human-infecting genotypes predominantly belonging to the Paslahepevirus balayani species (Hepeviridae family). HEV-1 and -2 are endemic in developing regions with an estimated 70,000 deaths annually.^{2,3} These infections occasionally result in fulminant hepatitis in pregnant women, with mortality rates reaching 20%-30%.4 Zoonotic HEV-3 and -4 cause sporadic autochthonous infections in developing and industrialized regions.² HEV-3 also causes chronic infections, especially in immunocompromised individuals, thereby increasing the risk of rapid progression to cirrhosis, graft loss and death.⁵ There is no approved specific antiviral therapy. The off-label use of ribavirin for chronic infection is associated with marked adverse effects and treatment failure. 6-8

HEV presents in two forms in infected hosts: quasienveloped (HEVenv⁺) and naked/nonenveloped particles (HEVenv⁻). During infection, HEVenv⁺ is released from the apical membrane into the bile duct, where the lipid envelope is presumably degraded by detergents and proteases in the bile, explaining the appearance of HEVenv in feces and bile. 10 While HEVenv⁺ circulates in the blood, HEVenv⁻ is presumed to be the main form responsible for transmission and is associated with higher infectivity. 11,12 In standard cell culture systems, intracellular HEV predominantly exists as HEVenv, while HEVenv⁺ is secreted into the supernatant.¹³ The HEV genome encodes three partially overlapping open reading frames (ORFs). 14 Open reading frame 2 (ORF2) encodes the major structural (ie, capsid) protein that can manifest in three

*These authors contributed equally to this work.

Abbreviations used in this paper: CHGA, Chromogranin A; DAPI, 4',6diamidino-2-phenylindole; HEV, hepatitis E virus; HIEs, human intestinal enteroids; Lgr5+, leucine-rich-repeat-containing G-protein-coupled receptor 5; ODM, organoid differentiation medium; OGM, organoid growth medium; ORF2, open reading frame 2; pe, postelectroporation; pi, postinfection; RT-qPCR, reverse transcription quantitative polymerase chain reaction; 3D, three-dimensional; 2D, two-dimensional; WGA, wheat germ agglutinin.



Most current article

Copyright © 2025 The Authors. Published by Elsevier Inc. on behalf of the AGA Institute. This is an open access article under the CC BY-NC-ND license (http://creativecommons.org/licenses/by-nc-nd/4.0/). 2772-5723

2

different forms: ORF2 is either assembled into infectious particles (referred to as ORF2i) and secreted via the exosomal pathway from infected hepatocytes, or secreted in glycosylated (ORF2g) and cleaved (ORF2c) forms not associated with infectious particles. ¹⁵

Numerous knowledge gaps remain on fundamental aspects of HEV infection and pathogenesis, partly due to challenges in HEV cultivation (*ie*, slow replication to low titers). ¹⁶ Since HEV is hepatotropic, the virus is typically propagated in vitro using liver-derived primary cells and hepatic immortalized cell lines. Despite HEV also being an enteric virus that is transmitted fecal-orally and shed in high titers in stool, the role and contribution of the gut in HEV-induced disease has received limited attention. HEV was shown to replicate in intestinal epithelial cells that release infectious particles, particularly from the apical side, which ribavirin failed to block, possibly explaining viral relapses observed in chronically infected patients.¹⁷ The gut epithelium was proposed to serve as the initial virus amplification site before dissemination to the liver, and acting as a reservoir, especially during chronic infections. ^{17,18} Yet, how the virus migrates from the gut to the liver is still not well understood. Moreover, a detailed understanding of HEV infection in the gut is still lacking, particularly concerning the specific intestinal cell types that are infected, the host response to the infection, the viral dissemination routes to extra-intestinal tissues (eg, kidney and central nervous system), and the disease-inducing mechanisms. Thus, new and more physiologically relevant cultivation models are needed to recapitulate the full tropism of HEV and illuminate missing details in HEV biology.

Organoid technology has the potential to advance knowledge in virus biology and host-pathogen interactions by providing a more physiologically relevant model. Notably, HEV replication in human liver-derived organoids has been reported.¹⁹ Human intestinal organoids closely mimic the human intestinal epithelium in vitro, making them valuable for dissecting virus-host interactions of several enteric viruses.²⁰⁻²⁵ Human intestinal organoids are nontransformed three-dimensional (3D) cell cultures arranged in a crypt-villus structure that incorporate the physiological features of the intestinal epithelium, including the presence of different cell populations (enterocytes, goblet cells, enteroendocrine and Paneth cells).²⁶ Intestinal organoids can be derived from induced pluripotent stem cells or tissue leucine-rich-repeat-containing G-proteincoupled receptor 5 (Lgr5+) stem cells, known as human intestinal enteroids (HIEs).27,28 We here used HIEs to establish an HEV infection model of the small intestine via various strategies and subsequently employed it to study HEV infection, including its cellular tropism in the gut.²⁹

Material and Methods

Human Intestinal Enteroid Culture

HIEs derived from fetal ileum (HT124), adult jejunum (J2) or adult small intestine (Lonza), were maintained at $37\,^{\circ}\text{C}$ with

 $5\%~CO_2$ in extracellular matrix (Matrigel, Corning) and IntestiCult Organoid Growth Medium (OGM; StemCell Technologies), that was replaced every other day. Differentiation was triggered by Wnt3a removal with IntestiCult Organoid Differentiation Medium (ODM; StemCell Technologies) for 5 days with medium changes every other day. HIEs culture and experimentation was performed under the approval of the Ethical Committee comite KU Leuven (approval number G-2024-8519-R2(AMD).

Cells

HepG2/C3A cells (ATCC CRL-10741) were cultivated in Dulbecco's Modified Eagle Medium (DMEM, Gibco), supplemented with 10% inactivated fetal bovine serum (FBS, Gibco), 2 mM L-glutamine (Gibco), 0.75 g/L sodium bicarbonate (Gibco) and 1 mM sodium pyruvate (Gibco). For seeding of HepG2/C3A cells, plates were coated with 100 μ g/mL rat tail collagen (Sigma-Aldrich) and 0.02 M glacial acetic acid in PBS for a minimum of 2 h at 37 °C. Subsequently, the plates were washed three times with PBS. PLC3, a subclone of PLC/PRF/5 hepatoma cells (CRL-8024), was cultured as previously described. 15

Viruses

HEV-3 full-length Kernow-C1 p6 infectious cDNA clone (GenBank accession number JQ679013) and its G1634R variant, containing the G1634R mutation in the viral polymerase, were previously detailed.⁶ The subgenomic Kernow-C1 p6/luc, with part of ORF2 replaced by the *Gaussia* luciferase gene, was constructed as described previously.³⁰ Similarly, the genotype 1 reporter replicon Sar55/s17/luc was derived from the HEV strain Sar55/s17 (GenBank accession number AF444002), as described earlier.³¹ The construction of plasmid pLA-B350/luc was previously reported.³²

Generation of Infectious Virus Stocks

Capped viral RNA was generated from the cDNA plasmids as previously described.⁸ In brief, Kernow-C1 p6, Kernow-C1 p6 G1634R, Kernow-C1 p6/luc, and pLA-B350/luc were linearized by MluI (Promega), while Sar55/s17/luc was linearized by BgIII (Promega). Subsequently, *in vitro* transcription was carried out using the Ribomax large-scale RNA production systems (Promega), and subsequent capping was performed using the ScriptCap m7G capping system (Cellscript), according to the manufacturer's protocols.

Kernow-C1 p6 or G1634R virus stocks were either a mixture of nonenveloped and enveloped virus (env $^{+/-}$), or only nonenveloped virus (env $^{-}$). In short, capped Kernow-C1 p6 or G1634R RNA was transfected into HepG2/C3A cells through electroporation as previously described. After 7 days of incubation, extracellular enveloped and intracellular nonenveloped Kernow-C1 p6 or G1634R were harvested as follows. For extracellular virus, supernatant was collected and centrifuged at 4000 rpm at 4 $^{\circ}$ C for 15 min, followed by the removal of cell debris, the concentration of the virus in the supernatant using minimate tangential flow filtration (100K pore size capsules, Pall Corporation), according to the manufacturer's protocol. For intracellular virus, electroporated cells were collected by trypsinization, resuspended in fresh

complete DMEM, and subjected to three freeze-thaw cycles in liquid nitrogen to release the virus from the cells. The lysate was subsequently centrifuged at 10,000xg for 10 min. Nonenveloped virus either or not mixed with concentrated enveloped virus was aliquoted and stored at $-80\,^{\circ}\text{C}$ until further use. Levels of infectious virus and viral RNA in the stock were determined by immunofluorescence staining using the HEV ORF2 protein and reverse transcription quantitative polymerase chain reaction (RT-qPCR), respectively, as previously described. Extracellular Kernow-C1 p6 virus from electroporated PLC3 cells was generated as previously described17 and used for the immunoprecipitation (IP) and gradients.

HEV Infection in 3D Enteroids

HEV infection of 3D-HIEs was performed as previously described for other enteric viruses with minor modifications.^{20,21,24} Briefly, 3D-HIEs were removed from matrigel, thoroughly washed with CMGF(-) medium (Advanced DMEM/F12 (Gibco) supplemented with GlutaMAX-1 2 mM (Gibco), HEPES 10 mM (Gibco), penicilin-streptomicin 100 U/mL (Gibco) and primocin 100 µg/mL (Invivogen), and gently fragmented. 3D-HIEs were resuspended in infection medium [ODM supplemented with 500 μM glycochenodeoxycholic acid (GCDCA; Sigma-Aldrich) and 10 μM Y-27632 (StemCell Technologies)] and inoculated with HEV or mock-infected. After virus inoculation, 3D-HIEs were incubated for 6 h at 37 °C with homogenization every hour. After, 3D-HIEs were washed with CMGF(-) (5x), resuspended in matrigel and plated in prewarmed 48-well plates (20 μ L drop containing 1.0 \times 10⁵ cells). After matrigel polymerization for 10 min at 37 °C, infection media [ODM supplemented with 500 μ M GCDCA, 10 μ M Y-27632 and 2 mM ruxolitinib (Toronto Research Chemicals)] was added to each well. At multiple timepoints post infection (pi), cells and supernatant were collected for RNA extraction. Infection of undifferentiated 3D-HIEs followed the same protocol with HIEs always cultured in OGM, including the infection medium.

HEV Infection in Transwell

Proliferating 3D-HIEs were collected and dispersed into single cells using TrypLE express (Gibco) and seeded on semipermeable transwell inserts (0.4 μ m PET membrane, avantor) that were precoated with collagen type IV (EMD Millipore). After 2 days in OGM, cells were maintained in ODM until formation of a polarized monolayer (6-7 days). Transepithelial electrical resistance of monolayers was measured using an epithelial voltohmmeter (World Precision Instruments). Polarized monolayers were infected with HEV Kernow-p6-G1634R through the apical side for 6 h at 37 °C. After, cells were washed five times with CMGF(-). ODM supplemented with 500 μ M GCDCA and 2 μ M ruxolitinib was added to the apical and basal compartments and incubated at 37 °C and 5% CO₂. Supernatant from the apical and basolateral sides, and cells from the apical side were harvested at multiple time points pi. Infection of undifferentiated two-dimensional (2D)-HIE monolayers followed the same protocol with HIEs always cultured in OGM, including the infection medium.

Enteroid Electroporation

HIE culture and preparation of single cell suspension was performed as described previously.³⁴ Briefly, fetal ileum

3D-HIEs were kept in OGM for 5 days. Forty-eight hours prior to electroporation, medium was replaced by ODM supplemented with 5 μ M CHIR99021 (StemCell technologies) and 10 μ M Y-27632. Twenty-four hours prior to electroporation, medium was replaced by ODM supplemented with 5 μ M CHIR99021, 10 μ M Y-27632% and 1.25% (V/V) dimethyl sulfoxide. HIE single cell suspensions were prepared using TrypLE express supplemented with 10 µM Y-27632 for 20 min at 37 °C. Single-cell suspensions of HIEs (1.0 \times 10⁶ cells) were resuspended in 200 μL BTX buffer (BTXpress; BTX Harvard Apparatus), mixed with 10 μg capped Kernow-C1 p6, Kernow-C1 p6-G1634R, Kernow-C1 p6/luc, Kernow-C1 p6 G1634R/luc, pLA-B350/luc, or Sar55/s17/luc RNA in a 4-mm (avantor) cuvette. An ECM 830 Electro Square Porator (BTX Harvard Apparatus) was used to deliver two pulses at 450 V for 2 msec with 100 ms interval between each pulse. The addition of viral RNA to the electroporation mixture was omitted for the cell control samples. Electroporated cells were incubated in ODM with 10 µM Y-27632 for 40 min at RT, then centrifuged and resuspended in 100% matrigel and plated in prewarmed 48-well plates (20 μL drop containing 1.0×10^5 cells). For immunofluorescence experiments, electroporated cells were resuspended in 50% matrigel-ODM solution and plated in black wall 96-well plates (Greiner) precoated with 5% matrigel. Electroporated cells were cultured in ODM supplemented with 10 μ M Y-27632, 5 μ M CHIR99021 (StemCell technologies) and 1.25% V/V dimethyl sulfoxide, either with or without ribavirin (Sigma-Aldrich).

Luminescence-Based Replicon Assay

To track the replication kinetics of luciferase expression activities in HIEs electroporated with HEV replicons carrying the luciferase gene, 20 μ L of culture medium was collected at various time points postelectroporation (pe). Luciferase activity was assessed via the Renilla luciferase kit (Promega). In brief, 20 μ L of the culture medium was transferred to white 96-well Culture Plates (PerkinElmer), followed by the addition of 50 μ L (1:100 diluted) *Gaussia* substrate. Luminescence produced by the secreted *Gaussia* luciferase was measured using a Spark microplate reader (Tecan).

Cell Viability

Enteroid viability was assessed using the Live-Dead Cell Viability Assay Kit (EMD Millipore) according to the manufacturer's instructions. Briefly, media was aspirated and replaced with dye mixture and incubate for 60 min at 37 $^{\circ}$ C. Images were acquired on a DMi8 (Leica) fluorescence microscope with a 10x objective.

RNA Extraction and Reverse Transcriptase Quantitative PCR (RT-qPCR)

Extracellular viral RNA was extracted from 50 or 150 μ L supernatant collected from infected/transfected HIEs or HepG2/C3A cells, by using the NucleoSpin RNA virus kit (Macherey-Nagel). For intracellular viral RNA, cells were harvested in TRIzol Reagent (Invitrogen) and RNA extracted with DirectZol RNA extraction kit (Zymo Research, R2051) according to manufacturer's instructions. HEV RNA loads were quantified using an established human HEV RT-qPCR protocol as previously described. 35,36

4 Santos-Ferreira et al

HEV RNAs for HEV particle characterization were extracted from 140 μ L culture supernatants using the QiAmp viral RNA mini kit (Qiagen). HEV RNA levels were quantified by RT-qPCR using the Takyon One-Step qPCR kit and using primers (5'-AAGA-CATTCTGCGCTTTGTT-3' (F) and 5'-TGACTCCTCATAAGCATCGC-3' (R)) and a probe (5'-FAM-CCGTGGTTCCGTGCCATTGA-TAMRA-3') targeting a conserved region of ORF1. RT-qPCR was performed on a QuantStudio 3 device.

Gene expression analysis of intestinal epithelial cell type mRNA levels was performed in samples harvested in TRI Reagent and extracted with DirectZol RNA extraction kit. An iTaq Universal SYBR Green One-Step Kit (Bio-Rad) was used to quantify the relative expression of different intestinal cells markers: Lgr5 (stem-cells), Lysozyme (Paneth cells), sucrose isomaltase (mature enterocytes), mucin 2 (goblet cells) and chromogranin A (CHGA; enteroendocrine cells), using specific primers as previously described. RT-qPCR was carried out in a QuantStudio 5 Real-Time PCR System (Applied Biosystems). GAPDH was used to normalize gene expression. Relative expression was determined using the $\Delta\Delta$ Cq method.

Immunofluorescence Staining and Focus-forming Assay

Immunofluorescence assays were performed at the peak of replication, ie, after day 11 pe, as described previously.²⁴ Briefly, supernatant was removed without disturbing the HIE layer and cells were fixated with a 2% paraformaldehyde (PFA) solution at 4 °C overnight. Then, cells were permeabilized (0.2% Triton X-100), blocked (1% goat serum and 3% bovine serum albumin (BSA) and incubated overnight with primary antibodies at 4 °C. Subsequently, cells were incubated with corresponding secondary antibodies (Invitrogen), followed by nuclear counterstaining with 4',6-diamidino-2-phenylindole (DAPI, Dilactate, Invitrogen) for 1 h at RT. The following antibodies or dyes were used: anti-ORF2 (HEV-specific rabbit hyperimmune serum), anti-Ki67 (EMD Millipore, MAB4190), antisucrose isomaltase (Santa Cruz techonology, sc-393424), anti-CHGA (Santa Cruz Biotechonology, sc-393941), phalloidin (Invitrogen, A12380) or wheat germ agglutinin (WGA, Vector laboratories, RL-1022). Images were acquired on an Andor Dragonfly 200 series High Speed confocal platform system (Oxford instruments, Abingdon, UK) at a 25× magnification connected to a Leica DMi8 microscope (Leica Microsystems, Wetzlar, Germany). Image processing was done with the Imaris analysis software (version 9.8.2). The 3D colocalization analysis of virus and intestinal epithelial cell markers was done using Imaris 3D colocalization software (voxel-based colocalization). Images are presented as maximum projections.

For high-content imaging experiments, immunofluorescence staining was performed using DAPI (blue), HEV ORF2 (green), Ki67 (red), CHGA (red) and Phalloidin CF660R (farred). Confocal microscopic images of the HIEs were acquired using an Operetta CLS High-Content Imaging and Analysis system (Revvity). A 20X water immersion objective was used to capture 16 planes in four different channels with an overal z-height of 15 μ m. Image analysis was performed on the maximum projection of the z-stacks using the Harmony software (Revvity). The phalloidin stained cell membrane was

used to identify the HIEs and downstream image analysis algorithms were used for the individual HIE segmentation and morphological feature extraction. Cell count was performed by counting the DAPI positive nuclei. Proliferative and enteroendocrine cells were counted based on positive Ki67 and CHGA signals, respectively, in close proximity of the DAPI stained nuclei. The presence of viral particles was detected by positively stained ORF2 and infected objects (HIEs, proliferative or enteroendocrine cells) were identified when both channels were positive.

For detecting HEV ORF2 in HepG2/C3A cells infected with HEV stocks, HepG2/C3A cells (7500 cells/well) were seeded in a 96-well plate with 10% complete DMEM the day prior to HEV infection. Viruses were serially diluted at 1:3, with a 1:6 dilution as the starting dilution. On day 7 pi, the cells were fixed with 3.7% PFA and incubated for 30 min at RT. Next, cells were permeabilized (0.1% Triton X-100) and blocked (3% BSA). Subsequently, the cells were incubated overnight at 4 °C with primary antibody anti-ORF2 (HEV-specific rabbit hyperimmune serum), followed by incubation with the secondary antibody goat antirabbit Alexa Fluor 488 (1:800, Thermo Scientific) and nuclear counterstaining with DAPI (1:800; Sigma-Aldrich) for 1 h. Fluorescent images of each well were acquired using a high-content imager (Arrayscan XTI, Thermo Fisher Scientific). Viral titers in focus-forming units were determined by counting the number of single HEV ORF2-positive cells through image analysis using the HCS Studio Cellomics software (Thermo Fisher Scientific, Version 6.6.2).

Immunoprecipitation (IP)

Antibodies recognizing the different forms of the HEV ORF2 protein, either P1H1 antibody recognizing the ORF2i form or P3H2 recognizing the three ORF2 forms (ORF2i, ORF2g, ORF2c) were used. 37 These antibodies as well as an IgG control antibody were coupled to Epoxy M-270 Dynabeads beads (Thermofisher) overnight at 37 °C. Beads were washed and incubated with either 0.5%-Triton treated supernatant (IP-P1H1 and an appropriate IgG control (Santa cruz biotechnology, sc-2025) or heat-inactivated supernatant (IP-P3H2 and an appropriate IgG control) for 1 hour at RT. Beads were washed six times and heated in Laemmli buffer. Proteins were separated by 10% sodium dodecyl sulfate-polyacrylamide gel electrophoresis and transferred onto nitrocellulose membranes, where detection of ORF2 proteins was done by using 1E6 monoclonal antibody (Millipore) and corresponding peroxidase-conjugated secondary antibodies, followed by exposure using the ImageQuant 800 chemiluminescent imaging system (Cytiva Life Sciences).

Density Gradient Analysis

Density gradient analysis was performed as previously described. ¹⁵ In brief, supernatants with equal HEV RNA copy numbers from PLC3/Kernow-C1 p6 and HIEs/Kernow-C1 p6 G1634R were layered on a preformed 7.5%–40% iodixanol gradient, followed by centrifugation for 16 hours at $160,000\times g$ at 4 °C, using a SW41 swinging-bucket rotor (Beckman Coulter). Twelve fractions of 1 mL were collected, and their density was measured by refractometry. The HEV RNA load was quantified by RT-qPCR as described above.

Statistical Analysis

Statistical analysis was performed using GraphPad Prism (version 10.2.0; GraphPad Software, Inc). All data were presented as mean + standard deviation (SD) of at least 3 independent experiments unless otherwise stated. The specific methods of statistical analysis and P values are indicated in the figure legends or the text.

Results

HEV Infection in Differentiated 3D Human Intestinal Enteroids is Limited

To investigate whether HIEs are permissive to HEV replication, fetal and adult differentiated 3D-HIEs were infected with wildtype HEV-3 Kernow-C1 p6 or Kernow-C1 p6 G1634R bearing a fitness-enhancing mutation⁶ (for simplicity, we will below refer to these as respectively 'HEV-3' and 'HEV-3^{G1634R}'), after which the viral load (derived from pooled cell extracts and supernatant) was assessed at different days postinfection (pi) (Figures 1A and A1). When using an inoculum of 1.0×10^7 HEV RNA copies, HEV-3 infection of either fetal or adult HIEs resulted in a very limited gain in HEV RNA over input (Figure 1B). Infection with higher titer HEV-3^{G1634R} (5.0×10⁷ RNA copies) yielded a modest increase of ~1 log₁₀ in HEV RNA

from 6 to 72 hours pi, after which levels remained stable until day 5 pi, albeit significant in adult HIEs (Figure 1C). Thus, a high inoculum may be required to kick-start the infection but results in no gain in replication.

HEV Infection in HIE Polarized Monolayers Leads to Higher Apical Viral Shedding

Next, we cultured HIEs as polarized monolayers (2D) in a transwell system, allowing us to study virus shedding into both the apical and basolateral compartments (Figure 2A). Prior to HEV infection, the transepithelial electrical resistance of the monolayers was measured at $>300 \Omega/\text{cm}^2$, indicating a tight and polarized intestinal epithelium. Infection of differentiated fetal or adult 2D-HIEs with the (slightly better replicating) HEV-3^{G1634R} led to a constant virus shedding (HEV RNA levels of $\sim 5.5 \log_{10}/\text{mL}$) to the apical side of the intestinal epithelial layer (Figure 2B). Basolateral shedding was also detected, albeit at lower levels of ~ 3.5 - 4 log₁₀ HEV RNA copies/mL (Figure 2B). Given that half of the culture media was replaced by fresh media in both compartments every 2 days, this result demonstrates that new virions were produced and shed into the culture supernatant. Intracellular HEV RNA levels remained around 5 log₁₀ copies/well with a slight drop over time (Figure 2C).

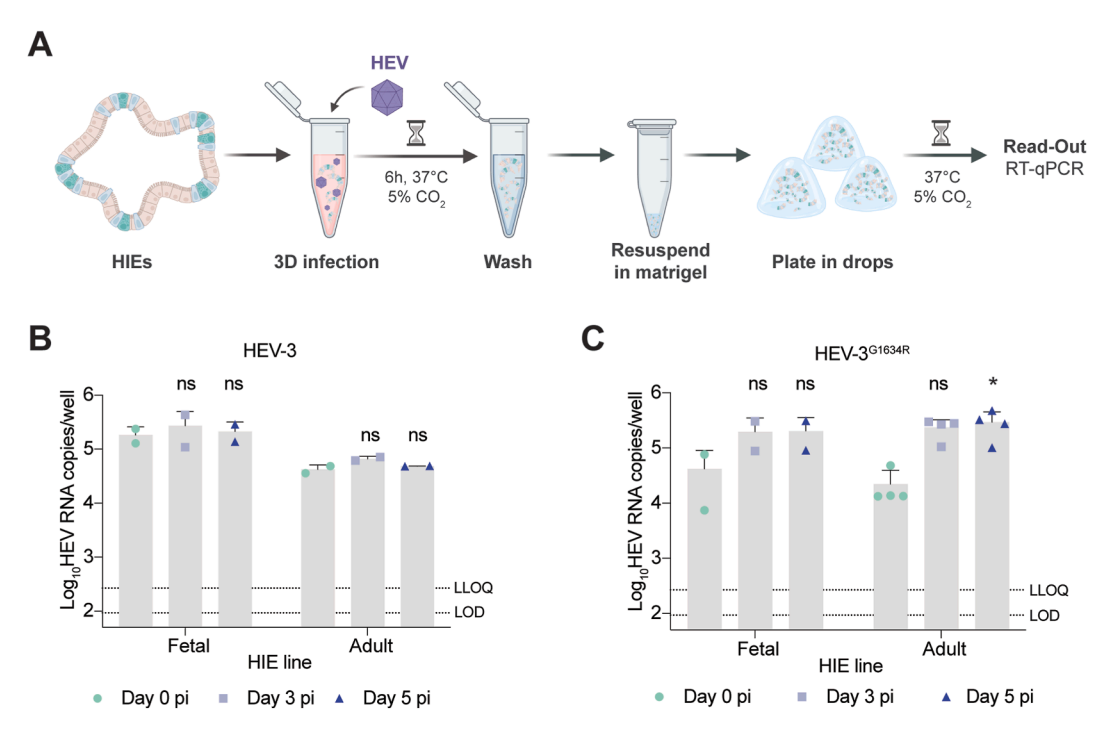


Figure 1. Establishment of HEV infection in the 3D-HIEs model. (A) Schematic representation of the experimental layout. (B) Fetal and adult differentiated 3D-HIEs were infected with HEV-3 (env⁻, 1.0×10^7 GEs) (N = 2). (C) Fetal (N = 2) or adult (N = 4) differentiated 3D-HIEs were infected with HEV-3^{G1634R} (env⁻, 5.0×10^7 GEs). HEV RNA of the whole well (pool of supernatant and cell lysate) was quantified by RT-qPCR. Day 0 pi represents 6 h pi. Data are mean + SD. *, P < 0.05. Statistical analysis was performed using two-way ANOVA followed by Tukey's test for multiple comparisons. GEs, genome equivalents; LLOQ, lower limit of quantification; LOD, limit of detection; pi, postinfection. Schematic representation created with BioRender.com.

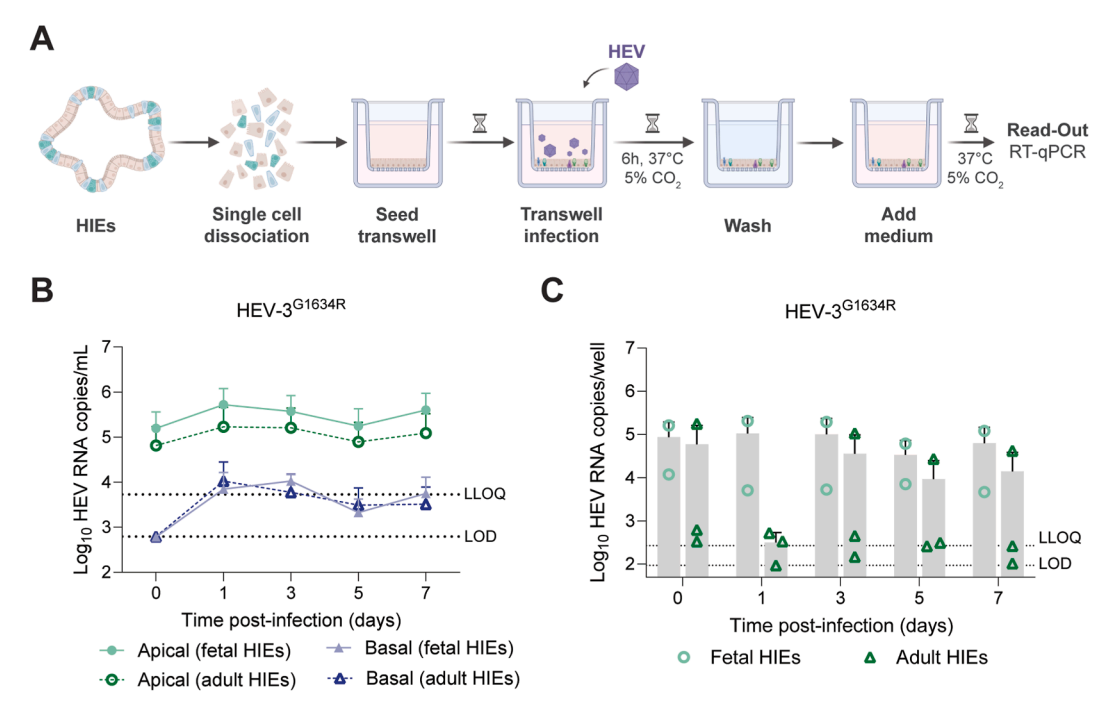


Figure 2. HEV infection dynamics in polarized 2D-HIEs in transwell system. (A) Schematic representation of the experimental layout. (B) Extracellular HEV released into apical or basal supernatant of fetal (N=2) or adult (N=3) differentiated 2D-HIEs infected with HEV-3^{G1634R} (env⁻, 2.0×10^8 GEs). Half of the medium ($100~\mu$ L apical and $300~\mu$ L basolateral compartment) was refreshed every 2 days. (C) HEV RNA levels in infected fetal (N=2) or adult (N=3) differentiated 2D-HIEs cell lysates. Day 0 pi represents 6 h pi. Data are mean + SD.

Robust HEV Replication in HIEs Electroporated With Capped Viral RNA

Next, we evaluated whether electroporation of a HIE single-cell suspension with capped viral RNA resulted in a more efficient HEV replication. Single cell HIEs were electroporated with subgenomic or full-length HEV capped RNA from human HEV-1 (Sar55/s17), HEV-3 (Kernow-C1 p6), HEV-3 G1634R (Kernow-C1 p6 G1634R), or rat HEV (pLA-B350), as illustrated in Figure 3A. HIEs electroporated with RNA of the luciferase-encoding subgenomic replicons HEV-3/luc, HEV-1/luc or rat HEV/luc yielded a 17-, 5- and 10-fold increase in luciferase levels, respectively, at the day of peak replication (day 4 pe for HEV-3/luc and rat HEV/luc, day 11 pe for HEV-1/luc) (Figure 3B). Ribavirin treatment resulted in lower luciferase signals compared to nontreated HIEs electroporated with HEV-3/luc, with a mean half-effective concentration of around 25 μ M (Figure 3C).

Electroporation with full-length HEV-3 or HEV-3^{G1634R} resulted in a sustained increase of the viral load in the supernatant over time, reaching 4.9×10^5 and 5.8×10^5 HEV RNA copies/mL, respectively, at day 15 pe (Figure 3D). Moreover, HIEs electroporated with HEV-3 or HEV-3^{G1634R} markedly expressed ORF2 antigens (Figure 3E). The percentage of infected cells was 36% and 57%, respectively, in HEV-3 and HEV-3^{G1634R} electroporated HIEs, with the peak replication at day 11 pe (Figures 3F and A2A–F), in line with viral RNA levels (Figure 3D). The single-cell electroporated HIEs proliferated and formed the characteristic 3D

organoids, translating in a significant increase in the cell number over time (Figure 3G). HIEs electroporated with HEV RNA, however, grew slower and the 3D structures were smaller compared to their mock-electroporated equivalents (Figure A2D and G). This difference is likely not due to cell death, as HEV-electroporated HIEs presented less propidium iodide positive staining than mockelectroporated HIEs (Figure A3). Ribavirin treatment of full-length HEV-3G1634R-electroporated HIEs resulted in a dose-dependent reduction in intracellular and extracellular HEV RNA levels (Figure A4), corroborating the earlier findings obtained with HIEs electroporated with HEV subgenomic RNA (Figure 3C). The toxicity of ribavirin was also evaluated in (mock-)electroporated fetal ileum HIEs, yielding a 50% cytotoxic concentration (CC₅₀) of 43.1 \pm 5.6 μ M (N=4). Incubation of HIEs with 50 μ M ribavirin resulted in reduced organoid size at day 11 pe and a marked increase in the cell death, as determined by livedead staining with propidium iodide (Figure A5).

Since HEV appears to preferentially infect proliferative cells, we investigated whether the higher HEV replication observed upon electroporation could be explained by the differentiation state of the HIEs. To this end, both differentiated and undifferentiated 3D- and 2D-HIEs were used in HEV infection experiments. To preserve the undifferentiated state, a subset of the HIEs was maintained in growth medium (OGM) rather than differentiation medium (ODM), thereby retaining the stem cell niche and associated

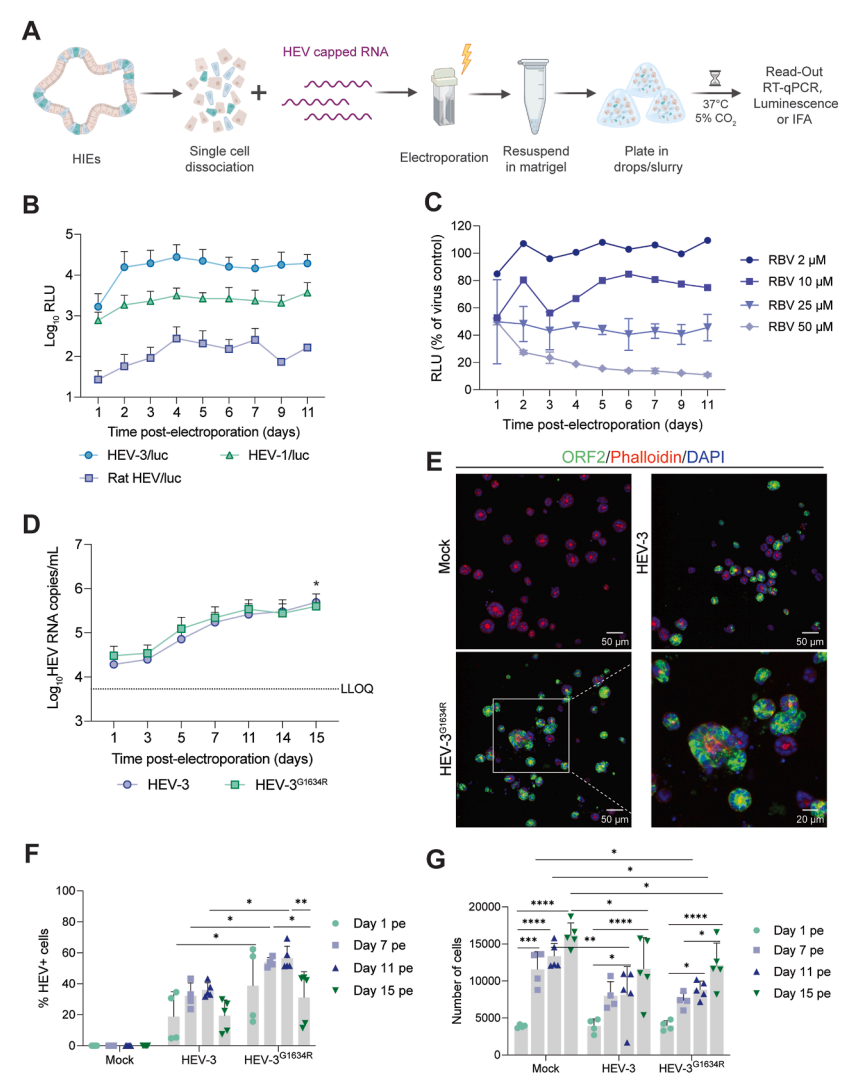


Figure 3. Electroporated HIEs allow robust HEV replication. (A) Schematic representation of the experimental layout. (B) Fetal ileum HIEs were electroporated with mock, HEV-3/luc (N = 6), HEV-1 HEV-1/luc (N = 2) or ratHEV/luc (N = 3) capped RNA. (C) HEV-3/luc electroporated fetal ileum HIEs treated with different RBV concentrations (N = 2). Viral replication related luciferase activity was determined in 20 µL supernatant up to day 11 pe. (D) Fetal ileum HIEs were electroporated with mock, HEV-3 (N=4) or HEV-3^{G1634R} (N=4) full-length capped RNA. Half of the medium was refreshed at day 11 pe. Viral replication was determined by RT-qPCR in 50 μ L supernatant up to day 15 pe. *P < .05 (calculated using two-way ANOVA followed by Tukey's test for multiple comparisons; comparing day 1 pe versus day 15 pe for either HEV-3 or HEV-3^{G1634R}). (E) Representative images of HEV ORF2 expression in HEV-3 or HEV-3 G1634R electroporated fetal ileum HIEs at day 11 pe. Immunofluorescence staining with ORF2 (HEV, green); Phalloidin (actin, red); and DAPI (nuclei, blue). Images were acquired on a Spinning-disk confocal microscope with a 25× objective. Scale bar – 50 or 20 μm. (F) Percentage of HEV ORF2 positive cells in mock-, HEV-3- or HEV-3^{G1634R}-electroporated fetal ileum HIEs at day 1, 7, 11 and 15 pe. The percentage of infected cells are defined as total number of cells containing ORF2 signal within the nucleous or in close proximity thereof divided by the number of total cells counted using the DAPI signals in the same well. (G) Number of cells in mock-, HEV-3 or HEV-3^{G1634R}electroporated fetal ileum HIEs at day 1, 7, 11 and 15 pe. Number of cells was determined by nuclear staining (DAPI) and enumerated by high-content imaging (HCI). Statistical analysis was performed using the 2-way ANOVA, followed by Tukey's multiple comparisons test. *, P < .05; **, P < .01; ***, P < .001; ****, P < .0001. pe, postelectroporation; RBV, ribavirin; RLU, relative luminescence unit. Data are mean+/±SD.

proliferation capacity. Infection of undifferentiated 3D-HIEs with HEV-3 $^{\rm G1634R}$ resulted in a more efficient first replication cycle (8.0 \times 10 $^{\rm 3}$ RNA copies in OGM versus 3.3 \times 10 $^{\rm 3}$ RNA copies in ODM) at day 1 pi (Figure A6A). Although this difference was significant, viral loads became similar at later time points.

Infection of undifferentiated 2D-HIEs in transwell resulted in a continuous apical virus release (Figure A6B), as was shown earlier for differentiated 2D-HIEs. Altogether, these results suggest that HEV replication is influenced by the differentiation state of HIEs at the onset of infection.



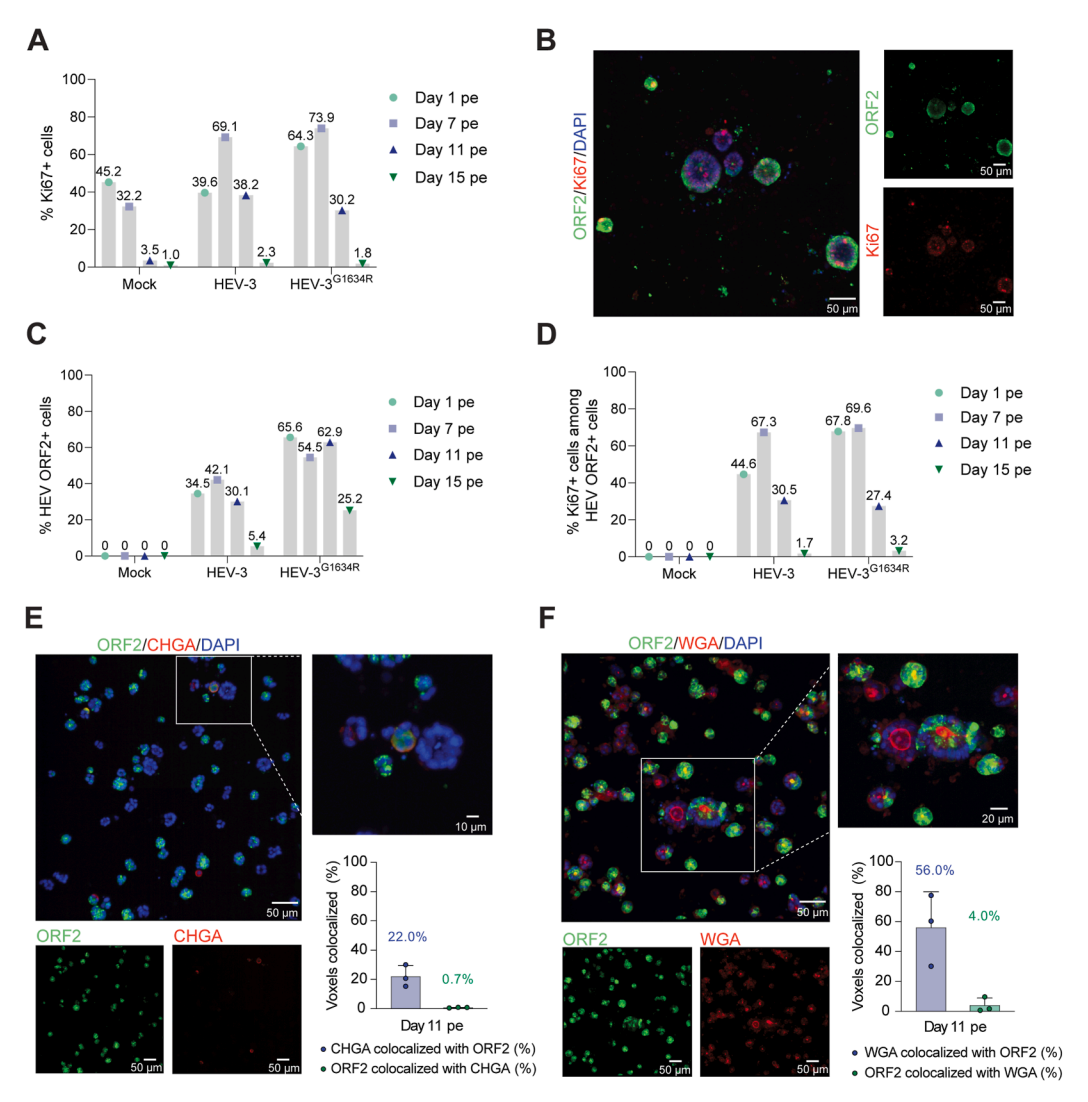


Figure 4. Targeted cell tropism of HEV in infected HIEs. (A) Percentage of proliferative cells in mock-, HEV-3 or HEV-3^{G1634R}electroporated fetal ileum HIEs at day 1, 7, 11 and 15 pe. Amount of proliferative cells was determined by HCl and defined by the objects positive for both DAPI and the proliferation marker Ki67. (B) Representative image of immunofluorescence staining of HEV-3^{G1634R} electroporated fetal ileum HIEs at day 11 pe. Cells were stained with HEV ORF2 (green) and Ki67 (red). (C) Percentage of HEV ORF2 capsid positive cells within the proliferative cell population in mock-, HEV-3 or HEV-3^{G1634R}-electroporated fetal ileum HIEs at day 1, 7, 11 and 15 pe. These cells were defined by the objects positive for all three markers (Ki67 and HEV ORF2). (D) Percentage of cells that were positive for proliferative marker (Ki67) within the HEV ORF2 positive population in mock-, HEV-3 or HEV-3 G1634R electroporated fetal ileum HIEs at day 1, 7, 11 and 15 pe. These cells were defined by the objects positive for all three markers (DAPI, Ki67 and HEV ORF2). (E, F) Representative images of immunofluorescence staining of HEV-3^{G1634R} electroporated fetal ileum HIEs at day 11 pe. Cells were stained with HEV ORF2 (green) and antibody specific for (E) enteroendocrine cells (CHGA, chromogranin A, red) or (F) goblet cells (WGA, wheat germ agglutinin). DAPI (blue) was used as counterstaining. Overlap of voxels between HEV ORF2 and (E) CHGA signal (N = 3, 8fields/experiment) or (F) WGA signal) (N = 3, 5 fields/experiment). pe, postelectroporation.

HEV Infects and Preserves the Proliferative Intestinal Stem Cell Niche

Next, we looked at the cellular composition of the HEVelectroporated HIEs and the permissiveness of various intestinal cell types to HEV infection. Electroporated HIEs were mainly composed of proliferating cells (Ki67+ cells), reaching 45% and 70% of the cell composition, in mock and HEV-electroporated conditions, respectively, in the first week (Figure 4A). Interestingly, the amount of proliferating cells decreased in mock-electroporated HIEs while it increased in HEV-electroporated HIEs during the first week after electroporation. When looking at the mRNA transcript levels of the intestinal epithelial cell markers, Lgr5+ (stem cells), lysozyme (Paneth cells), sucrose isomaltase (mature enterocytes), mucin 2 (goblet cells) and CHGA (enteroendocrine cells), a similar increase in transcript levels was found in HIEs electroporated with HEV-3 and HEV-3 G1634R as well as for mock-electroporated HIEs (Figure A7),

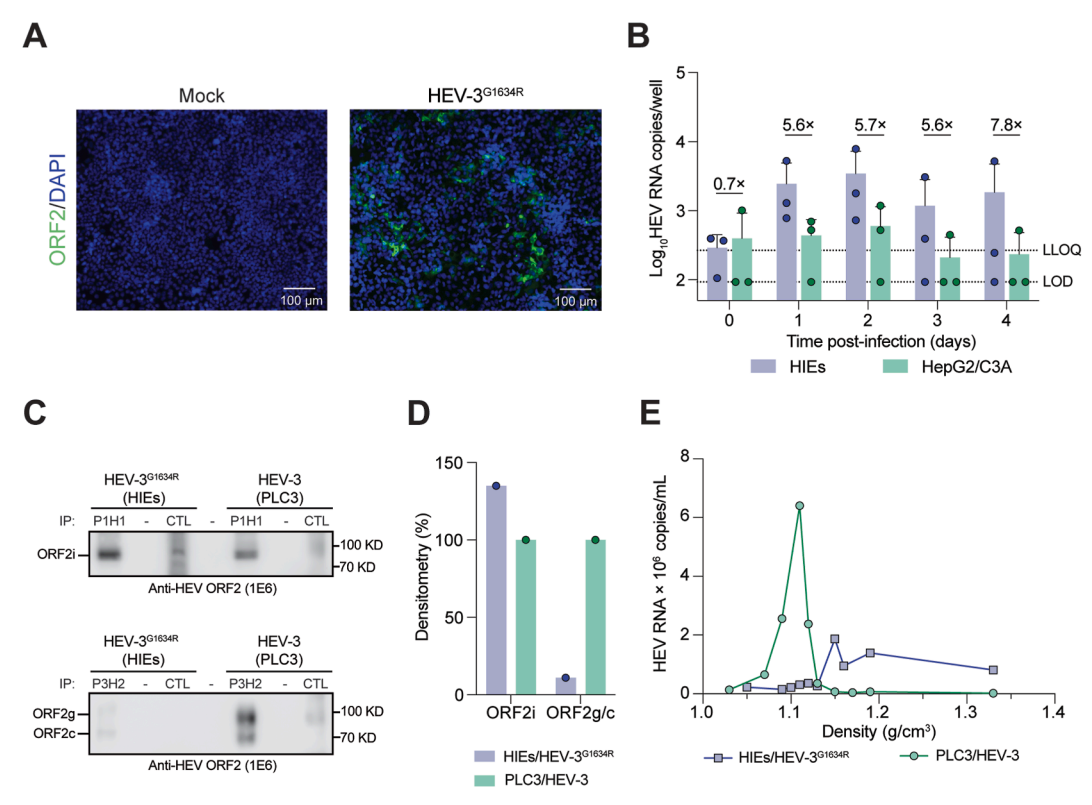


Figure 5. Characterization of HEV particles produced in HEV-electroporated HIEs. (A) Representative images of HEV ORF2 immunofluorescence staining in HepG2/C3A cells infected with the supernatant of HEV-3^{G1634R} electroporated HIEs (HIEs/HEV-3^{G1634R}, 1:6 dilution) (N = 3). Uninfected HepG2/C3A cells served as negative control. Scale bar – 100 μm. ORF2 (green); DAPI (blue). Images acquired on a DMi8 microscope (Leica) with a 10× objective. (B) Proliferating fetal ileum 3D-HIEs were infected with 1.0×10^6 GEs HEV produced in HIEs/HEV-3^{G1634R} or in HepG2/C3A cells (env⁻) (N = 3). HEV RNA levels in the whole well were quantified by RT-qPCR. Day 0 pi represents 6 h pi. Data are mean + SD. Fold changes in viral load were determined by comparing HIEs-derived infections against HepG2/C3A-derived infections at each time point (illustrated within the histogram). Statistical analysis was performed using the 2-way ANOVA, followed by Tukey's multiple comparisons test. (C) Expression of different forms of ORF2 protein (ORF2i, ORF2g, ORF2c) in supernatant of HIEs/HEV-3^{G1634R} and PLC3/HEV-3, as determined by immunoprecipitation using two different antibodies (P1H1 and P3H2) followed by western blot analysis. (D) Densitometry plot of band intensity, % HIEs compared to PLC3. (E) Density gradient of HIEs/HEV-3^{G1634R} and PLC3/HEV-3 supernatant. CTL, IP-negative controls.

suggesting that HEV infection had no effect on the proliferative cell niche, while enabling differentiation of mature cell types, *ie*, enterocytes, goblet and enteroendocrine cells. Furthermore, the differentiation of 3D-HIEs and 2D-HIEs resulted in a decrease in Lgr5+ mRNA transcript levels, reflecting a reduction in intestinal stem cells, and detection of fewer Ki67+ cells (Figure A8).

Confocal imaging of immunofluorescent staining of virus and cell markers showed that proliferating cells, *ie*, positive for the proliferation marker Ki67, were positive for HEV ORF2 protein expression (Figures 4B, A9 and A10A) and with up to 42% and 55% of the proliferating cells found to be infected with HEV-3 or HEV-3^{G1634R}, respectively, on day 7 pe (Figure 4C). From all HEV-infected cells, almost 70% were proliferating cells (Figure 4D).

We also examined whether mature intestinal epithelial cell types were infected. HEV ORF2 signal was detected in enteroendocrine cells (CHGA) (Figures 4E and A10B). Colocalization of virus with CHGA showed that 0.7% of the

thresholded HEV ORF2 signal colocalized with the CHGA signal, while 22.0% of the thresholded CHGA signal overlapped with the ORF2 signal (Pearson coefficient of 0.092). Moreover, ORF2 expression was also detected in cells containing mucins (mucin staining with WGA), indicating that HEV is able to infect goblet cells (Figure 4F). Colocalization analysis showed that 4.0% of the thresholded HEV ORF2 signal colocalized with WGA signal, while 56.0% of the thresholded WGA signal overlapped with the ORF2 signal (Pearson coefficient of 0.190). Most enterocyte-specific antibodies (including sucrose isomaltase, SI) stain the apical surface, making colocalization studies challenging. However, given that enterocytes are the major cell type of the intestinal epithelium and that infected HIEs display an expanded and intense ORF2 signal (Figure A10C), including cells that form the brush borders (as visualized by Phalloidin staining in Figure 3E), it is most likely that enterocytes are targeted by HEV. Overall, the HEV ORF2 capsid protein was expressed in proliferating, absorptive as well as secretory cells.

10

HEV-Electroporated HIEs Produce Infectious HEV Particles that Are Nonenveloped

We next infected HepG2/C3A cells with supernatant from HEV-electroporated HIEs (referred to as HIEs/HEV-3^{G1634R}, collected on day 11 pe, Figure 5A) to confirm the infectivity of the virions shed in the supernatants of HIEs/ HEV-3^{G1634R}. Indeed, the infected HepG2/C3A cells markedly expressed HEV ORF2 antigens on day 7 pi, resulting in a titer of 4.0×10^6 focus forming units per mL (N = 3). Moreover, viral replication was more efficient when proliferating 3D-HIEs were infected with HIEs/HEV-3^{G1634R} than with HepG2/C3A-HEV-3^{G1634R} (intracellular-derived virus stock, HEVenv⁻). In particular, at the peak of replication (day 2 pi), the viral load was 5.7 times higher when using the HIEs-derived HEV stock than when using the HepG2/C3A-derived HEV stock (P = .0679) (Figure 5B). To further characterize the type of HEV virions being released from the HIEs/HEV- 3^{G1634R} , HIEs electroporated with viral RNA were cultured in in-house ODM (BSA-free) for 11 days, followed by the analysis of the ORF2 forms present in the supernatant by IP and western blot (Figure 5C and D), and density gradient centrifugation (Figure 5E). Using the P1H1 antibody that specifically recognizes the particle-associated ORF2i form,³⁷ an intense band corresponding to the ORF2i protein was detected in the HIEs/HEV-3^{G1634R} supernatant (Figure 5C, left part in the top panel). Interestingly, the amount of ORF2i proteins in HIEs/HEV-3G1634R supernatant was ~1.4-fold higher than in the supernatant of human hepatoma PLC3 cells electroporated with HEV-3 RNA ('PLC3/HEV-3') control samples (Figure 5C, right part in the top panel and 5D). Conversely, IP with the P3H2 antibody, which recognizes ORF2g/c forms,³⁷ resulted in poor detection of the secreted glycosylated ORF2g/c forms in the HIEs/HEV-3^{G1634R} supernatant, unlike in PLC3/HEV-3derived virus (Figure 5C, bottom panel and 5D). Density gradient analysis of the HIEs/HEV-3G1634R supernatant showed high levels of HEV RNA in fractions 9, 10, and 11 that corresponded to HEV particles with densities of 1.15-1.19 g/cm³ (Figure 5E), which are typical of nonenveloped particles, 15,17 thus indicating that viral particles released from HIEs/HEV-3^{G1634R} are mostly naked.

Discussion

HEV has been recognized as enterically transmitted since the late 1970s, ³⁸ yet evidence supporting its infection of the gut has remained limited, which is partly due to its relatively inefficient *in vitro* cultivation. Understanding HEV infection in the primary infection site, the gut, as well as HEV dissemination to the liver is essential to grasp HEV pathogenesis. In addition, identifying the intestinal cellular tropism of HEV should offer novel insights into virus-host interactions and potential disease mechanisms, which are highly relevant for an efficient clinical management and for the development of novel therapeutics. The development of human intestinal organoids has transformed the *in vitro*

cultivation of various enteric viruses,³⁹⁻⁴¹ hence holding great potential for HEV, which is considered a slow-growing, hard-to-cultivate virus.

There are several methods to deliver infectious organisms into organoid cultures. 42 In this study, we explored three different ways to infect HIE cultures with HEV.²⁹ HEV was able to replicate in fetal and adult differentiated 3D-HIEs in an input-dependent manner. However, replication was somewhat limited, with a constant viral load detected until day 5 pi. Similar results were obtained when infecting 2D-differentiated HIE monolayers. The sustained high HEV viral load generated, despite the frequent medium changes, is comparable in terms of replication kinetics to what is observed in hepatocyte-like immortalized models,³³ primary hepatocytes¹² and liver organoids.¹⁹ Given that HEV is a slow replicating virus, prolonging the assay may likely result in a higher replication yield. However, this was not feasible because of the differentiated state of the cells and the consequent accumulation of debris in the lumen of the 3D organoid structure, resulting in loss of viability past this timepoint. In the 2D-HIE setup, HEV infection predominantly led to apical release of the virus, as demonstrated by a lower basolateral shedding. This indicates that access to the apical surface was not the limitation for efficient replication in 3D-HIEs. Moreover, these data, which are in line with previously described results using primary intestinal epithelial cells, 17 suggest that new HEV virions may be continuously excreted into the intestinal lumen.

Electroporation of single cell HIEs with HEV capped RNA proved to be the most effective method, leading to high viral yields, like with what is reported for human hepatocyte cell lines. 12 Hence, this approach is well suited for exploring the pathways that are involved in HEV infection of the gut. Many factors may be preponderant for successful HEV infection and/or further dissemination. The HEV replication cycle remains poorly understood, particularly its entry into host cells, which may be different based on the type of virus particle, host cell, and many other factors. 43,44 One obvious advantage of electroporation is that it overcomes the early steps of entry and uncoating. Still, a marked increase in viral load became evident only after 3 days pe. This observation suggests that the increase in viral load may also be linked to slower processes such as cell proliferation and may be the result of multiple replication cycles after infection.

In this model the enhanced replication of the HEV-3^{G1634R} variant was recapitulated, since it contains a fitness-enhancing mutation in the RNA-dependent RNA polymerase.¹² We further tested the efficacy of the antiviral ribavirin in the HIE-HEV electroporation model. Given that the gut could serve as an important reservoir for HEV,¹⁷ it is critical to evaluate (yet-to-be-developed) treatments against HEV in the gut. In this model, ribavirin effectively reduced viral RNA levels, both intra- and extracellularly, demonstrating that the model is amenable to evaluate the efficacy of novel therapeutic approaches in the intestinal compartment. The model also reproduced the known toxic

effects of ribavirin previously reported both *in vitro* and *in vivo* settings.⁴⁵

HEV-electroporated HIEs exhibited delayed growth (when compared to mock-infected), but an increase in the number of proliferative cells was observed. While mature cell types are present in all HIE culture types (including 3Dand 2D-HIEs), only the undifferentiated HIE single-cells had an elevated proportion of proliferative cells (ie approximately 40%). Moreover, the fact that nearly 70% of HEVinfected cells were proliferative cells indicates that this cell type better supports HEV replication, when compared to mature cell types. Of note, the fact that electroporation of single-cell HIEs is performed is an important factor that facilitates the first round of infection. However, the increase in viral load over 11 days, in parallel with increasing numbers of proliferative cells during infection, is highly suggestive that infection of this cell type is a determining factor for HEV sustained and highly efficient replication in these cultures. It would be relevant to directly compare this to electroporation of single-cell differentiated HIEs but these cells are, however, not viable after electroporation.

Infection of undifferentiated 3D-HIEs suggests that HEV replication is influenced by the differentiation state of HIEs at the onset of infection (*ie*, day 1 pi). Yet, at later timepoints we do not see a difference anymore, perhaps due to the limited space for cell expansion. The 3D-HIEs are already of a certain size when they are fragmented during infection, after which they rapidly reform their 3D structures and gradually differentiate. By electroporating single cell HIEs with HEV, we have the combined advantage of accelerating the first replication cycle while providing ample opportunity and nutrients for the HIEs to expand.

The infection of mature cell types may have additional implications regarding HEV infection and disease. Infection of enterocytes is a finding that is not surprising as HEV can replicate in Caco-2 cells. Enteroendocrine cells are estimated to comprise approximately 1% of the intestinal epithelial cell population, serving as sensory sentinels of the intestinal environment and possessing rich endocrine functions. HEV infection of enteroendocrine cells could explain the early symptoms in HEV-infected individuals, such as vomiting. Similar findings were reported for the enteric human rotavirus, which causes acute gastroenteritis and also infects enteroendocrine cells, inducing serotonin release to the basolateral side of the epithelium, which consequently stimulates vagal afferent nerves and the vomiting center in the brain. 48,49

One important aspect in HEV biology is the characterization of the shed virions from infected tissues to determine whether they are naked or quasienveloped. Density gradient centrifugation showed that infectious HEV virions released by infected HIEs were naked. Since naked virions are associated with a higher infectivity, ¹² their presence likely facilitated further dissemination of progeny virions to new cells, hence explaining the higher viral titer of the HEV stock derived from electroporated HIEs as well as the higher amounts of expressed ORF2i proteins. Moreover,

infection of 3D-HIEs with HIEs/HEV-3^{G1634R} yielded a higher virus replication, most likely due to the higher infectivity of the inoculum that mainly contains naked virions. This finding is novel and contrasts with a previous study that detected mainly quasienveloped virus shed by human primary intestinal cells.¹⁷ Likewise, HEV egress from liver cell cultures is reported to occur in the quasienveloped form.⁵⁰

We here postulate that while HEV can infect virtually all intestinal cell types, infection of proliferative cells is key for a more productive and sustained infection of the gut, likely due to an efficient production of naked virions in these cells. This is based on the following observations: 1) only HIEs cultures used for electroporation present high proportion of proliferative cells; 2) a marked increase in HEV RNA levels after electroporation happened over a period of 11 days, implying that a more efficient multiple-replication cycle process is taking place; 3) the virions produced in electroporated HIEs are mainly naked, which supports the notion of a more efficient replication, also because reinfection of new HIEs happens with rapid replication kinetics (ie peaking at 48 h and yielding higher HEV RNA levels). In contrast, when differentiated HIEs in 3D or 2D were used (where few to no proliferative cells are left), lower and constant HEV RNA levels were reached. Likewise when human intestinal primary cells were used by Marion et al., 17 cultures likely did not contain proliferative cells anymore, thereby yielding quasienveloped virions to be produced. Therefore, efficient production of naked virions (which can better infect new cells) is a key feature to obtain an overall increase in viral load overtime; a process not occurring in cultures in which insufficient proliferative cells are present and infected.

This hypothesis also suggests that virus progeny produced by HEV-infected mature (nonproliferative) cell types may consist mainly of quasienveloped virions, which are less efficient in infecting new cells and thus resulting in lower and steady HEV RNA levels over time. Further studies are needed to understand how intracellular processes differ between infected proliferative and non-proliferative intestinal cells. Along the same line, additional studies utilizing different intestinal segments from various donors would provide a more thorough characterization of HEV replication and shedding in the intestine.

In conclusion, we established an efficient infection model for HEV using intestinal organoids. Direct delivery of HEV RNA to single-cell HIEs that continued to develop into 3D-HIEs resulted in high levels of infectious naked virions. We discovered that HEV is able to infect multiple types of intestinal cells, mainly proliferative cells. By contrast, lower HEV RNA yields were detected when fewer or no proliferative cells were present and infected. Thus, the fast epithelial cell turnover of the gut, with direct infection of proliferative cells, is key for establishing a highly productive HEV infection of the gut, likely impacting viral dissemination within and beyond this organ towards the liver. Overall, this work demonstrates the relevance of the

12

gut as an HEV reservoir, suggesting that part of the naked HEV shed in the feces originates directly from this organ.

Supplementary Materials

Material associated with this article can be found, in the online version, at https://doi.org/10.1016/j.gastha.2025. 100769.

References

- Purdy MA, Drexler JF, Meng XJ, et al. ICTV virus taxonomy profile: hepeviridae 2022. J Gen Virol 2022; 103:1–2.
- Raji YE, Toung OP, Taib NM, et al. Hepatitis E virus: an emerging enigmatic and underestimated pathogen. Saudi J Biol Sci 2022;29:499–512.
- 3. Rein DB, Stevens GA, Theaker J, et al. The global burden of hepatitis E virus genotypes 1 and 2 in 2005. Hepatology 2012;55:988–997.
- Chaudhry SA, Verma N, Koren G. Hepatitis e infection during pregnancy. Can Fam Physician 2015; 61:607–608.
- Ma Z, de Man RA, Kamar N, et al. Chronic hepatitis E: advancing research and patient care. J Hepatol 2022; 77:1109–1123.
- Debing Y, Gisa A, Dallmeier K, et al. A mutation in the hepatitis e virus RNA polymerase promotes its replication and associates with ribavirin treatment failure in organ transplant recipients. Gastroenterology 2014; 147:1008–1011.e7.
- Todt D, Walter S, Brown RJP, et al. Mutagenic effects of ribavirin on hepatitis E virus-viral extinction versus selection of fitness-enhancing mutations. Viruses 2016; 8:1–15.
- Debing Y, Ramière C, Dallmeier K, et al. Hepatitis E virus mutations associated with ribavirin treatment failure result in altered viral fitness and ribavirin sensitivity. J Hepatol 2016;65:499–508.
- 9. Kamar N, Izopet J, Pavio N, et al. Hepatitis E virus infection. Nat Rev Dis Prim 2017;16:1–16.
- Takahashi M, Yamada K, Hoshino Y, et al. Monoclonal antibodies raised against the ORF3 protein of hepatitis e virus (HEV) can capture HEV particles in culture supernatant and serum but not those in feces. Arch Virol 2008; 153:1703–1713.
- 11. Yin X, Ambardekar C, Lu Y, et al. Distinct entry mechanisms for nonenveloped and quasi-enveloped hepatitis E viruses. J Virol 2016;90:4232–4242.
- Todt D, Friesland M, Moeller N, et al. Robust hepatitis e virus infection and transcriptional response in human hepatocytes. Proc Natl Acad Sci U S A 2020; 117:1731–1741.
- Takahashi M, Tanaka T, Takahashi H, et al. Hepatitis e virus (HEV) strains in serum samples can replicate efficiently in cultured cells despite the coexistence of HEV antibodies: characterization of HEV virions in blood circulation. J Clin Microbiol 2010;48:1112–1125.
- Lhomme S, Marion O, Abravanel F, et al. Clinical manifestations, pathogenesis and treatment of hepatitis E virus infections. J Clin Med 2020;9:1–25.

- Montpellier C, Wychowski C, Sayed IM, et al. Hepatitis E virus lifecycle and identification of 3 forms of the ORF2 capsid protein. Gastroenterology 2018;154:211–223.e8.
- Meister TL, Bruening J, Todt D, et al. Cell culture systems for the study of hepatitis E virus. Antivir Res 2019; 163:34–49.
- Marion O, Lhomme S, Nayrac M, et al. Hepatitis e virus replication in human intestinal cells. Gut 2020;69:901–910.
- 18. Oechslin N, Moradpour D, Gouttenoire J. Hepatitis E virus finds its path through the gut. Gut 2020;69:796–798.
- Li P, Li Y, Wang Y, et al. Recapitulating hepatitis E virushost interactions and facilitating antiviral drug discovery in human liver-derived organoids. Sci Adv 2022;8:1–17.
- Mirabelli C, Santos-Ferreira N, GillillandIII MG, et al. Human norovirus efficiently replicates in differentiated 3D-Human intestinal enteroids. J Virol 2022;96: e0085522.
- 21. Santos-Ferreira N, Van Dycke J, Chiu W, et al. Molnupiravir inhibits human norovirus and rotavirus replication in 3D human intestinal enteroids. Antivir Res 2024;223: 105839.
- 22. Kolawole AO, Mirabelli C, Hill DR, et al. Astrovirus replication in human intestinal enteroids reveals multicellular tropism and an intricate host innate immune landscape. PLoS Pathog 2019;15:1–30.
- Holly MK, Smith JG. Adenovirus infection of human enteroids reveals interferon sensitivity and preferential infection of goblet cells. J Virol 2018;92:1–15.
- 24. Masmoudi F, Santos-Ferreira N, Pajkrt D, et al. Evaluation of 3D human intestinal organoids as a platform for EV-A71 antiviral drug discovery. Cells 2023;12:1–14.
- 25. Lamers MM, Beumer J, van der Vaart J, et al. SARS-CoV-2 productively infects human gut enterocytes. Science 2020;369(80):50–54.
- 26. Sato T, Stange DE, Ferrante M, et al. Long-term expansion of epithelial organoids from human colon, adenoma, adenocarcinoma, and Barrett's epithelium. Gastroenterology 2011;141:1762–1772.
- 27. Günther C, Winner B, Neurath MF, et al. Organoids in gastrointestinal diseases: from experimental models to clinical translation. Gut 2022;71:1892–1908.
- 28. Taelman J, Diaz M, Guiu J. Human intestinal organoids: promise and challenge. Front Cell Dev Biol 2022;10:1–9.
- 29. Santos-Ferreira N, Zhang X, Van Dycke J, et al. Proliferative cell targeting and epithelial cell turnover fuels hepatitis E virus replication in human intestinal enteroids. bioRxiv 2024.
- Shukla P, Nguyen HT, Faulk K, et al. Adaptation of a genotype 3 hepatitis E virus to efficient growth in cell culture depends on an inserted human gene segment acquired by recombination. J Virol 2012;86:5697–5707.
- Emerson SU, Zhang M, Meng XJ, et al. Recombinant hepatitis E virus genomes infectious for primates: importance of capping and discovery of a cis-reactive element. Proc Natl Acad Sci U S A 2001; 98:15270–15275.
- Debing Y, Mishra N, Verbeken E, et al. A rat model for hepatitis E virus. DMM Dis Model Mech 2016; 9:1203–1210.
- Meister TL, Klöhn M, Steinmann E, et al. A cell culture model for producing high titer hepatitis e virus stocks. J Vis Exp 2020;2020:1–19.

- Fujii M, Matano M, Nanki K, et al. Efficient genetic engineering of human intestinal organoids using electroporation. Nat Protoc 2015;10:1474–1485.
- Debing Y, Emerson SU, Wang Y, et al. Ribavirin inhibits in vitro hepatitis E virus replication through depletion of cellular GTP pools and is moderately synergistic with alpha interferon. Antimicrob Agents Chemother 2014; 58:267–273.
- Zhang X, Cremers N, Hendrickx S, et al. Establishment of a robust rat hepatitis E virus fecal-oral infection model and validation for antiviral studies. Antivir Res 2023;216: 105670.
- Bentaleb C, Hervouet K, Montpellier C, et al. The endocytic recycling compartment serves as a viral factory for hepatitis E virus. Cell Mol Life Sci 2022;79:1–25.
- 38. Lemon SM, Walker CM. Enterically transmitted non-a, non-b hepatitis and the discovery of hepatitis E virus. Cold Spring Harb Perspect Med 2019;9:1–14.
- Foulke-Abel J, In J, Kovbasnjuk O, et al. Human enteroids as an ex-vivo model of host-pathogen interactions in the gastrointestinal tract. Exp Biol Med 2014;239:1124–1134.
- Ramani S, Crawford SE, Blutt SE, et al. Human organoid cultures: transformative new tools for human virus studies. Curr Opin Virol 2018;29:79–86.
- Kolawole AO, Wobus CE. Gastrointestinal organoid technology advances studies of enteric virus biology. Plos Pathog 2020;16:1–7.
- 42. Blutt SE, Estes MK. Organoid models for infectious disease. Annu Rev Med 2022;73:167–182.
- 43. Yin X, Feng Z. Hepatitis e virus entry. Viruses 2019; 11:1–10.
- 44. Brüggemann Y, Frericks N, Richter E, et al. How hepatitis E virus invades hepatocytes: the mystery of viral entry. Trends Microbiol 2025;33:866–874.
- 45. Noshy MM, Hussien NA, El-Ghor AA. Evaluation of the role of the antioxidant silymarin in modulating the in vivo genotoxicity of the antiviral drug ribavirin in mice. Mutat Res - Genet Toxicol Environ Mutagen 2013;752:14–20.
- Emerson SU, Nguyen H, Graff J, et al. In vitro replication of Hepatitis E Virus (HEV) genomes and of an HEV replicon expressing green fluorescent protein. J Virol 2004;78:4838–4846.
- 47. Worthington JJ, Reimann F, Gribble FM. Enteroendocrine cells-sensory sentinels of the intestinal environment and orchestrators of mucosal immunity. Mucosal Immunol 2018;11:3–20.
- 48. Hagbom M, Istrate C, Engblom D, et al. Rotavirus stimulates release of serotonin (5-HT) from human enterochromaffin cells and activates brain structures involved in nausea and vomiting. PLoS Pathog 2011;7:1–10.
- 49. Bialowas S, Hagbom M, Nordgren J, et al. Rotavirus and serotonin cross-talk in diarrhoea. PLoS One 2016;11:1–25.
- 50. Das A, Rivera-Serrano EE, Yin X, et al. Cell entry and release of quasi-enveloped human hepatitis viruses. Nat Rev Microbiol 2023;21:573–589.

Received May 14, 2025. Accepted August 20, 2025.

Correspondence:

Address correspondence to: Joana Rocha-Pereira, Virus-Host Interactions & Therapeutic Approaches (VITA) Research Group, Rega Institute, Herestraat 49, Box 1050, KU Leuven, Leuven 3000, Belgium. e-mail: joana.rochapereira@ kuleuven.be. Suzanne J. F. Kaptein, Virology, Antiviral, and Vaccine Research Group, Rega Institute, Herestraat 49, Box 1050, KU Leuven, Leuven 3000, Belgium. e-mail: suzanne.kaptein@kuleuven.be.

Acknowledgments:

We thank Prof. Luc Verschaeve (formerly at the Scientific Institute of Public Health, Belgium), Prof. Jason Spence (University of Michigan Medical School, United States) and Prof. Mary Estes (University of Michigan Medical School, United States) for providing the HepG2/C3A cells, fetal ileum HIEs and adult jejunum HIEs, respectively. We thank Prof. Suzanne Emerson (formerly at the National Institute of Allergy and Infectious Diseases, National Institutes of Health, United States) for kindly provide the plasmids Kernow-C1 p6, Kernow-C1 p6/luc, and Sar55/s17/luc. We also thank Prof. Eike Steinmann (Ruhr University, Germany) for the anti-ORF2 HEV-specific rabbit hyperimmune serum. We thank Joost Schepers (KU Leuven, Belgium) for the kind assistance with the high-content imaging analysis. We truly thank Dr Martin Ferrié (KU Leuven, Belgium) for all the insightful discussions.

GenBank accession number JQ679013, AF444002, KM516906.

Authors' Contributions:

Nanci Santos-Ferreira: Conceived and designed the study; performed experiments and analyzed data under the supervision of L.Coc., S.J.F.K., and J.R. P.; wrote the original manuscript; made critical revision of the manuscript for important intellectual content; read and approved the final manuscript. Xin Zhang: Conceived and designed the study; performed experiments and analyzed data under the supervision of L.Coc., S.J.F.K., and J.R.P.; wrote the original manuscript; made critical revision of the manuscript for important intellectual content; read and approved the final manuscript. Laura Corneillie: Performed experiments and analyzed data under the supervision of L.Coc., S. J.F.K., and J.R.P.; made critical revision of the manuscript for important intellectual content; read and approved the final manuscript. Jana Van Dycke: Made critical revision of the manuscript for important intellectual content; read and approved the final manuscript. Winston Chiu: Performed image acquisition and image analysis of high-content imaging experiments; read and approved the final manuscript. Claire Montpellier: Performed experiments and analyzed data under the supervision of L.Coc., S.J.F.K., and J.R.P.; read and approved the final manuscript. Johan Neyts: Made critical revision of the manuscript for important intellectual content; read and approved the final manuscript. Laurence Cocquerel: Made critical revision of the manuscript for important intellectual content; read and approved the final manuscript. Suzanne J. F. Kaptein: Conceived and designed the study; made critical revision of the manuscript for important intellectual content; read and approved the final manuscript. Joana Rocha-Pereira: Conceived and designed the study; made critical revision of the manuscript for important intellectual content; read and approved the final manuscript.

Conflicts of Interest:

The authors disclose no conflicts.

Funding

This work was partly supported by the Horizon 2020-funded ITN program OrganoVIR (Grant 812673) to N.S.F.; J.R.P. was supported by the KU Leuven Starting Grant STG/21/028. X.Z. was supported by the China Scholarship Council (grant no. 201906170033). L.Cor. was supported by the ANRS-MIE (ECTZ246976). J.V.D. was supported by the EU (DT-NMBP-23). W.C. research was performed using the "Caps-It" research infrastructure (project ZW13-02) that was financially supported by the Hercules Foundation (FWO) and Rega Foundation, KU Leuven.

Ethical Statement:

Human intestinal enteroids were originated in another laboratory and transferred to us under MTA agreement and to which we have ethical approval from the Ethics Committee Research UZ/KU Leuven (G-2024-8519-R2(AMD).

Data Transparency Statement:

The appropriate datasets will be made publicly available upon publication.

Reporting Guidelines:

Not applicable for this article type.